Article

Primary N_2–He gas field formation in intracratonic sedimentary basins

https://doi.org/10.1038/s41586-022-05659-0

Received: 19 April 2022

Accepted: 13 December 2022

Published online: 1 March 2023

Check for updates

Anran Cheng[1]✉, Barbara Sherwood Lollar[2], Jon G. Gluyas[3] & Chris J. Ballentine[1]✉

Helium, nitrogen and hydrogen are continually generated within the deep continental crust[1–9]. Conceptual degassing models for quiescent continental crust are dominated by an assumption that these gases are dissolved in water, and that vertical transport in shallower sedimentary systems is by diffusion within water-filled pore space (for example, refs. [7,8]). Gas-phase exsolution is crucial for concentrating helium and forming a societal resource. Here we show that crustal nitrogen from the crystalline basement alone—degassing at a steady state in proportion to crustal helium-4 generation—can reach sufficient concentrations at the base of some sedimentary basins to form a free gas phase. Using a gas diffusion model coupled with sedimentary basin evolution, we demonstrate, using a classic intracratonic sedimentary basin (Williston Basin, North America), that crustal nitrogen reaches saturation and forms a gas phase; in this basin, as early as about 140 million years ago. Helium partitions into this gas phase. This gas formation mechanism accounts for the observed primary nitrogen–helium gas discovered in the basal sedimentary lithology of this and other basins, predicts co-occurrence of crustal gas-phase hydrogen, and reduces the flux of helium into overlying strata by about 30 per cent because of phase solubility buffering. Identification of this gas phase formation mechanism provides a quantitative insight to assess the helium and hydrogen resource potential in similar intracontinental sedimentary basins found worldwide.

Helium (He) generated within the continental crust is an important societal resource and is also used as a natural tracer to determine fluid origin and residence in, for example, proposed geological carbon storage and nuclear waste repositories. Co-produced gases, hydrogen (H_2) and nitrogen (N_2), provide an energy resource and key nutrients that define the limits to subsurface life[1–7]. The continental crust produces ^{4}He and associated radiogenic noble gases by the decay of uranium (U) and thorium (Th) (for example, refs. [8,9]). H_2 is generated by associated groundwater radiolysis as well as the hydration of mafic or ultramafic rocks[4,5,10]. N_2 is always an important component in helium-rich (>0.1% helium) natural gases[11–17]; however, the mechanisms linking helium, a radiogenic gas, to nitrogen, radiochemically and physiochemically derived from minerals, in the crystalline continental crust have not been unambiguously resolved[12–19].

In stable cratons, these gases accumulate within the basement crystalline rock fracture network, in some cases on billion-year timescales[20–22]. Crustal He, nevertheless, escapes, with a global mean flux of 2.2×10^{-6} mol ^{4}He m^{-2} yr^{-1} (ref. [23]), comparable to the rate of He production of the whole crust of 1.47×10^{-6} mol ^{4}He m^{-2} yr^{-1} (refs. [20,24,25]). The distribution of He in pore fluids of overlying sedimentary lithologies is broadly consistent with cross-lithology transport by diffusion in water-filled medium, modified by advective lateral flow in some more permeable lithologies[1,7,20,26,27]. Larger fluxes occur in regions of high heat flow such as Yellowstone or the East African Rift, which accelerates the release of the deep accumulated crustal gases[23,28].

He itself as a non-renewable natural resource has recently been in short supply, historically discovered only serendipitously during hydrocarbon exploration[29–31]. Although He is relatively insoluble in groundwater, it is generated slowly. Reaching concentrations that cause gas-phase formation in the subsurface is a critical requirement to concentrate He and form a commercially viable resource (typically >0.1% He; ref. [6]). The presence of gases, such as methane (CH_4) and carbon dioxide (CO_2), can 'strip' dissolved He from the groundwater system[12,32], but these also serve to dilute the primary deep-crustal gases. Observed N_2–He-dominated gases contain higher He concentrations (percent level) and are probably formed from little-diluted primary deep-crustal gases[6]. Here we present a quantitative approach that identifies the processes and conditions that enable a primary deep-crustal gas phase to form in a sedimentary system and, in turn, develop an understanding of how this gas-phase formation impacts the regional basinal dissolved-gas diffusional flux.

Helium and nitrogen transport

The first consideration is recognition of the crucial role that the sedimentary basin architecture plays in promoting or impeding gas transport. Crustal He accumulation in shallower aquifers can provide a mean fluid residence time estimate when there is substantial lateral water migration and discharge[1,20,26,27]. By contrast, within some deeper basinal sedimentary sequences, lateral fluid migration may be

[1]Department of Earth Sciences, University of Oxford, Oxford, UK. [2]Department of Earth Sciences, University of Toronto, Toronto, Ontario, Canada. [3]Department of Earth Sciences, Durham University, Durham, UK. ✉e-mail: anran.cheng@earth.ox.ac.uk; chris.ballentine@earth.ox.ac.uk

limited (for example, ref. [33]) and vertical helium diffusional transport over longer periods becomes dominant[7]. In the latter case, the basinal evolution of the temperature, porosity, permeability and thickness of each stratigraphic lithology becomes important in building up high He concentrations in sedimentary pore fluids proximal to the underlying crystalline basement. However, He alone cannot sustain concentrations high enough in the sedimentary pore fluids, in even the deepest lithologies, to form a free gas phase[7].

The co-occurrence of N_2 with He provides the second critical consideration. Multiple sources of N_2 gas exist in sedimentary basins[12,13], with natural gas $N_2/^4He$ ratios in stratigraphic units distal from the crystalline basement ranging from hundreds to thousands[14–17]. He-associated N_2 has been unambiguously identified in the He-rich Hugoton Panhandle giant gas field (United States) with a basement $N_2/^4He$ ratio observed between 20 and 50 (ref. [12]). Whether the N_2 is released from low-grade metamorphic[12] or radiolytic routes[18,19], regional $N_2/^4He$ and local variance will be a function of mineral N_2 content, and U and Th concentration and age.

$N_2/^4He$ ratios observed in multiple sedimentary systems in gas fields proximal to the crystalline basement nevertheless show a relatively small range, between 6 and 59 globally. These include Sichuan Basin[34], Alberta Basin[16], Salina and Anardarko basins[35], Appalachian Basin[36], Southwestern Ontario Basin[36] and Amadeus Basin[13] (Extended Data Table 1). The co-occurrence of N_2, at concentrations 6–59 times higher than He, provides the potential to exceed the local pore-water gas saturation limit and form a free gas phase.

Modelling gas-phase formation

The He concentration of water-filled pore spaces within a sedimentary basin dominated by vertical He diffusion is sustained by: (1) the concentration gradient generated by the crystalline basement He flux into the base of the sedimentary system; (2) in situ He production from local sediment U + Th; and (3) He loss at the top surface of the sedimentary system (Methods). Pore-fluid He concentrations increase as a function of depth and lithology until the rate of He input reaches the rate of He top-surface loss (steady state). Steady state is perturbed on the timescale of the formation of new sedimentary sequences and does not always recover between depositional events[7]. Like He, a N_2 gradient in the water-filled pore space is also generated by the basement flux. This provides the chemical gradient for diffusive N_2 transport and is calculated for He as different sedimentary strata develop (Fig. 1a and Methods). The approach is further adapted to consider the solubility limit of N_2 and the effect of gas-phase formation when exceeded (Fig. 1b and Methods).

The upper concentration limit of N_2 in pore water in these calculations is controlled by its saturation solubility, which is a function of temperature, pressure and salinity[37]. When exceeded, a N_2 gas phase forms in the sedimentary unit. N_2 gas-phase formation partitions other pore-water-dissolved gases from the water into the new gas phase, including He (and H_2 if present), and provides a mechanism to generate a He-rich gas phase in such sedimentary units. As the N_2 solubility limit cannot be exceeded, continuing gas flux from the basement contributes further to gas-phase accumulation, increasing the gas–water volume ratio (Supplementary Video 1). This, in turn, controls the proportion of dissolved He and any H_2 partitioning into the gas phase. In our calculations, the initial N_2 concentrations in water-filled pore spaces are set to air-saturated-water values (Methods) for all geological units on deposition and are calculated iteratively as a function of depth and sediment formation with time. Although there can be multiple sedimentary sources of N_2 (for example, ref. [12]), or other co-generated gases such as H_2 (ref. [5]), the model here only considers He-associated N_2 from the crystalline basement. As such, the calculated results are conservative, as gas-phase formation would occur earlier if additional sedimentary-sourced N_2 or other gas sources such as H_2, CH_4 or CO_2, are substantial.

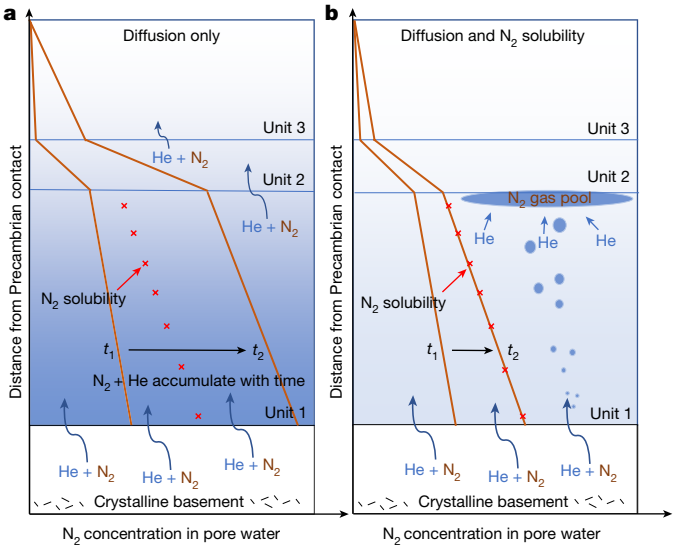

Fig. 1 | A schematic illustration of the concentration gradients (not to scale) of diffusion-controlled gases in pore water. a,**b**, The *y* axis shows sedimentary units overlying the crystalline basement and pore-water-dissolved N_2 concentration (*x* axis) changes as a function of time (t_1 and t_2). **a**, Considering diffusion only. **b**, Gas-phase formation caused when the N_2 solubility limit (crosses in **a**) is reached. Diffusion calculations (Methods) consider: (1) deposition of each sedimentary unit from the start of its geological age; (2) porosity and tortuosity change with compaction; (3) increasing pressure, temperature and salinity; and (4) steady-state ^4He and N_2 flux from the crystalline basement. The schematic concentration of He at t_2 is illustrated with the background colour; the darker the colour, the higher the concentration. Without considering N_2 solubility, N_2 and He diffuse through sedimentary units vertically into the shallower units (**a**). Integrating the effects of N_2 solubility shows both N_2 gas pool formation and how the solubility limit buffers gas concentration and reduces diffusive flux into overlying formations (Supplementary Video 1).

The Williston Basin is a classic intracontinental sedimentary basin straddling the United States/Canada border. Brine compositions and the hydraulic head in the centre of the basin have been used to argue that the deepest formations have not been disturbed since the deposition of Silurian evaporites at about 420 million years ago (Ma)[33]. The basinal flux estimated to account for the observed He concentration profile in the Williston Basin fluids across multiple stratigraphic units ranges between 0.8×10^{-6} mol ^4He m^{-2} yr^{-1} and 1.6×10^{-6} mol ^4He m^{-2} yr^{-1} (Fig. 2a), comparable to steady-state crustal He production and release[7]. Considering now the addition of a crystalline N_2 basement flux, calculations (Methods) show that N_2 solubility is exceeded in the pore fluids proximal to the crystalline basement if the crystalline basement He flux has a $N_2/^4He$ ratio between 25 and 50 (Fig. 2b). This is consistent with the observation of N_2–He-dominated gases recovered from the Wood Mountain well drilled into Cambrian sandstone (Deadwood Formation)[38,39], and within the wide range observed for the crystalline basement (0.05–1,240; Extended Data Table 1).

Importance of nitrogen gas-phase formation

Exsolution and N_2 gas-phase formation is a critical process resulting in He and N_2 concentration profiles in the groundwater that are lower relative to a diffusion-only model (Fig. 3). For example, in the model with a He flux of 1.6×10^{-6} mol ^4He m^{-2} yr^{-1} and $N_2/^4He$ flux ratio of 50 for 500 Ma, modern dissolved ^4He concentrations in the Deadwood Formation are reduced by 19–32% and dissolved N_2 concentrations are reduced by 2–50% relative to the models that do not incorporate exsolution. This is because when the N_2 solubility limit is reached, further increases in

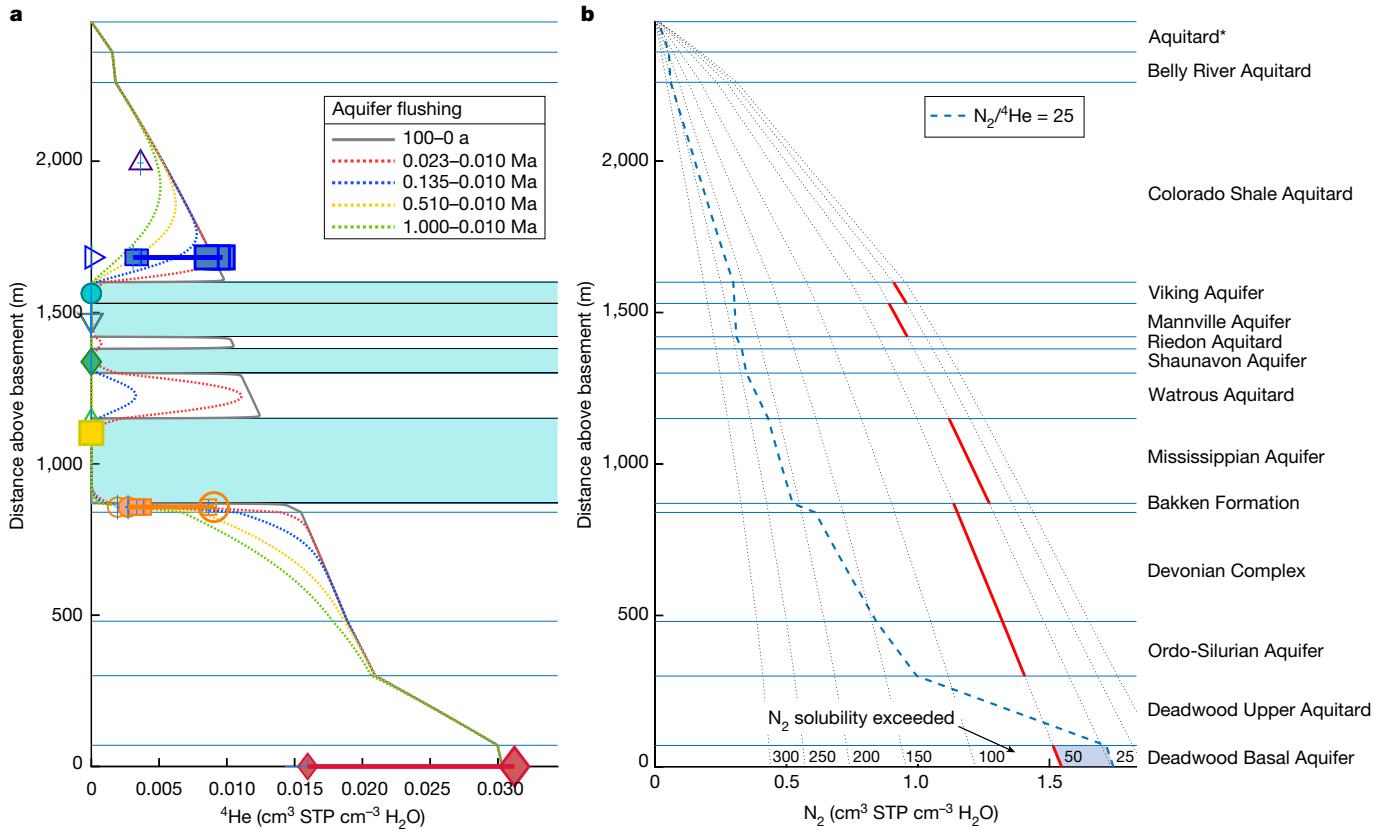

Fig. 2 | The Williston Basin groundwater concentration profiles of He and N_2 from diffusion-only models. a, Williston Basin diffusion-only model He groundwater concentration profiles, assuming a basement flux of 1.6×10^{-6} mol ^{4}He m^{-2} yr^{-1}, converge with observations (coloured symbols) when recent shallow aquifer (blue shaded areas) flushing is considered[7]. Aquifer flushing was modelled to simulate the impact of aquifer recharge driven by glaciation or anthropogenic water flooding during hydrocarbon production[7]. 100–0 a indicates modern aquifer flushing, from 100 years ago to current; 0.023–0.010 Ma indicates an aquifer flushing event between 0.023 million years ago and 0.010 million years ago, and so on. The horizontal lines are the lithological unit boundaries. Samples connected by a tie-line show before and after air correction, marking minimum and maximum He concentrations in the groundwater[7]. **b**, An example of the diffusive-only profiles (without exsolution) of N_2 concentrations assuming a basement flux of 1.6×10^{-6} mol ^{4}He m^{-2} yr^{-1} and a $N_2/^4$He basement flux ratio of 25 (Methods). The dotted black lines are the solubility of N_2 for different salinity, labelled to the right of each line. The solid red lines represent the solubility for different formation waters estimated from salinity maps produced by ref. [43]. The N_2 concentration of the Deadwood Basal Aquifer exceeds its solubility in this modelling scenario, predicting the formation of a N_2-rich gas phase. The geological unit names are marked to the right of panel **b**. Aquitard* refers to younger units collectively deposited above Belly River Aquitards, including quartenary glacial deposits.

the groundwater N_2 concentration cease in the lithology hosting the gas phase (phase solubility buffering). Gas-phase formation thus results in lower N_2 concentration gradients with depth and, therefore, lower rates of upwards N_2 diffusion compared with a diffusion-only scenario. The formation of a gas phase, therefore, also has a crucial effect on the He concentration gradient in the water column, which, in turn, controls the rate of upwards He diffusion. The formation of a gas phase critically influences the diffusional transport through the gas-forming unit and results in lower pore-water He and N_2 concentrations in shallower units due to the accumulation of gas-phase He in deep lithologies. Qualitatively, approaches that consider only diffusion may underestimate the basement He flux or conversely overestimate the local flux into the base of a lithological unit above a gas-bearing system.

When the N_2 gas-phase generation is not considered (diffusion-only model), N_2 concentrations greater than the saturation limit are predicted in multiple lithological units. The inclusion of exsolution in the model highlights the importance of considering gas-phase formation, which acts as an in-lithology sink for both He and N_2 that would have previously been dissolved in the water column. If there are no additional gas sources within the different lithologies, gas-phase formation at depth reduces the probability of gas-phase formation in units higher up in the stratigraphic section. However, shallower gas-phase accumulations of thermogenic and biogenic methane, sedimentary N_2 and magmatic CO_2 provide an additional mechanism to strip accumulated He from the water phase[12,32]. These can provide commercially useful albeit lower gas-phase concentrations of He.

The model result is consistent with the N_2-dominated He field observed close to the basement contact in the Williston Basin (Fig. 3). Mass-balance calculations suggest that for the Deadwood Formation, with a basement flux between 0.8×10^{-6} mol ^{4}He m^2 yr^{-1} and 1.6×10^{-6} mol ^{4}He m^2 yr^{-1}, a $N_2/^4$He flux ratio of 50 and in situ production from U + Th, 0.03–6% of the total ^{4}He influx over 500 Ma of basin history could be in the gas phase, 1–2% in the water phase and 93–98% lost to units above by diffusion (Fig. 4). Other studies from the Williston Basin report similar N_2-dominated gas fields in the same formation with gas compositions of 97% N_2 and 2% He (refs. [38,40]). On the flank of the Sweetgrass Arch, the Red River Formation (Ordovician) overlying the magma-intruded Cambrian layer has 95.5% N_2 with 0.98% ^{4}He (ref. [39]). Also, in the Williston Basin, He (0.1–0.2%) is reported in younger formations (for example, Milk River and Second White Specks formations of Cretaceous age). The shallower He-bearing gases all co-exist with CH_4 (>88%), which suggests that sedimentary CH_4 sources, in this case, play a notable role in the mechanism of exsolution in the shallower stratigraphic units, in addition to N_2.

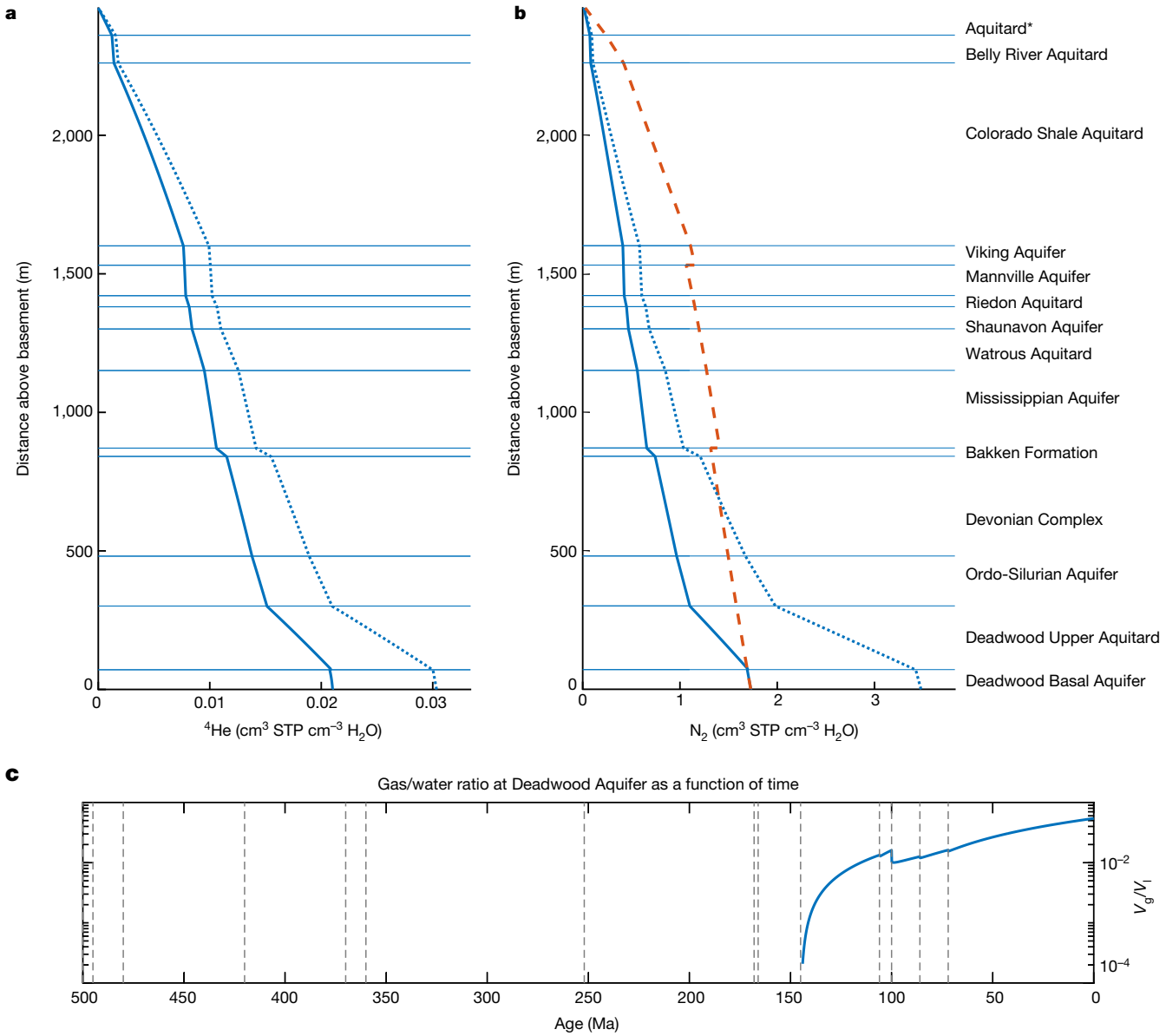

Fig. 3 | An example of the diffusion and exsolution model applied to the Williston Basin. The model is run for 500 Ma with a He flux of 1.6×10^{-6} mol ^{4}He m^{-2} yr^{-1} and a $N_2/^4$He flux ratio of 50. **a**, Concentration profile of ^{4}He calculated from the diffusion-only model and the diffusion–exsolution model. **b**, Concentration profile of N_2 simulated from the diffusion-only model and the diffusion–exsolution model. The solid lines represent He and N_2 profiles resulting from the diffusion–exsolution model. The dotted lines represent the diffusion-only profiles shown in Fig. 2. The red dashed lines in the N_2 profiles demonstrate the estimated solubilities for different sedimentary units. **c**, Gas–water volume ratio (V_g/V_l) of the Deadwood Basal Aquifer throughout geological time. The deposition time of different sedimentary units is marked as dashed lines. A gas phase is predicted to form at about 140 Ma (Supplementary Video 1). The decrease in V_g/V_l at about 90 Ma is due to an increase in basin pore-fluid pressure caused by the deposition of the Colorado Shale.

Previous work[7] has shown the impact of a history of recent water flooding and produced water disposal in some shallower lithologies (Fig. 2a). Here our approach rather involves a test of the sensitivity of our calculations for predicting gas-phase formation timing and location over longer timescales by theoretically re-setting all formation water dissolved-gas concentrations to background air-saturated-water levels at arbitrary points in time. This effectively simulates a complete 'flush' of the entire sedimentary column with air-saturated water and determines how quickly at that point in the sedimentary basin evolution the dissolved-gas concentration recovers to eventually reach saturation. With the basin evolution starting at 500 Ma, we test re-set scenarios at 300 Ma, 200 Ma and 100 Ma. Calculations show a weak dissolved-gas accumulation memory in the basin, resulting in gas-phase formation only being delayed from 145 Ma (no re-set) to 143 Ma, 131 Ma and 65 Ma for re-sets at 300 Ma, 200 Ma and 100 Ma, respectively (Methods). We conclude that the formation of a N_2-dominated He gas phase close to the basement is insensitive to hydrogeological events before 200 Ma, and that the system is still prone to gas-phase formation in the event of more recent perturbations. This is because the accumulation of the dissolved gases in the deepest units is most efficient when the sediment column above the deepest units is thick enough to be compacted and shield diffusive loss effectively.

N_2-dominated He reservoirs close to the basement contact observed in other sedimentary basins have already been noted (Extended Data Table 1). There are also examples of N_2-dominated He-rich gases in younger or shallower lithologies. In some of these, such gases may be

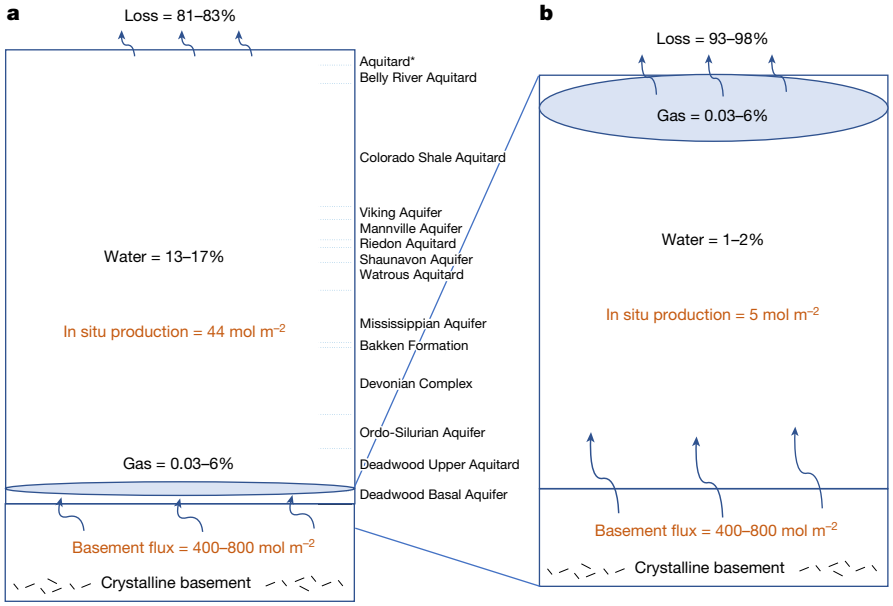

Fig. 4 | Mass balance of He distribution in the sedimentary column and the Deadwood Formation. a,**b**, Mass balance of He distribution in the sedimentary column (**a**) and the Deadwood Formation (**b**) assuming a basement flux between 0.8×10^{-6} mol ^{4}He m^{-2} yr^{-1} and 1.6×10^{-6} mol ^{4}He m^{-2} yr^{-1} (ref. [7]) and a $N_2/^4$He flux ratio of 50 over 500 Ma of basin history. The total basement flux of ^{4}He is between 400 mol m^{-2} and 800 mol m^{-2}. This compares with the flux from the total in situ ^{4}He production for the Deadwood Basal Aquifer and the sedimentary column since deposition of between 5 mol m^{-2} and 44 mol m^{-2}, respectively. For the entire sedimentary column, 0.03–6% of the total ^{4}He influx partitions into the gas phase, 13–17% is in the water phase and 81–83% is lost to the atmosphere. For the Deadwood Basal Aquifer, 0.03–6% of the total ^{4}He influx is in the gas phase, 1–2% is in the water phase and 93–98% is lost to units above by diffusion.

formed due to the presence of an unconformity bringing younger lithological units closer to the basement than modelled in the Williston Basin example. For example, in the Powder River Basin in Niobrara County in Wyoming (2°–40° N, 61° W), the Pennsylvanian strata are between less than 20 m and slightly over 100 m above the Precambrian basement[41], containing a reported 60.9% N_2 and 1.5% He (ref. [42]). In other cases, regional uplift could result in decompression and exsolution, which are not considered in the Williston Basin analysis here. For example, at Harley Dome, the Entrada Formation (Jurassic), situated 300 m above the Precambrian basement, has been uplifted owing to the reactivation of the Uncompahgre Fault and contains a reported 84% N_2 and 7.03–7.18% ^{4}He (ref. [39]). These examples suggest that N_2-dominated He fields are also formed through additional mechanisms that enhance the conditions necessary for gas-phase formation.

Impact of crustal degassing and gas reservoir formation

Primary He-rich gas fields, such as those discovered at the base of the Williston Basin Palaeozoic column and commonly observed in other major sedimentary basins globally, can be accounted for by steady-state crustal degassing and appropriate basin architecture. Calculations here, using a time-stepped one-dimensional diffusion and exsolution model with a basement He flux of 0.8–1.6×10^{-6} mol ^{4}He m^{-2} yr^{-1} and a $N_2/^4$He ratio of 25–50, typical for continental settings, predict gas-phase He concentrations and $N_2/^4$He matching those observed. This work demonstrates the importance of basement-sourced N_2 as the major exsolving gas phase and its control on the timing and location of He-rich gas reservoir formation in intracratonic and tectonic stable sedimentary basins. This mechanism is also important for the accumulation of H_2 sourced from basement rocks but requires an additional layer of complication because of the chemical reactivity and biological availability of H_2. The formation of a N_2- and He-rich gas phase is also shown to play a moderating role in the transport of dissolved components upwards through the stratigraphic section. This is by limiting the maximum He and N_2 concentration in the water phase, thereby buffering the concentration gradient that controls upwards N_2 and ^{4}He diffusion. The accumulation of gases in deep sedimentary units close to the basement is not sensitive to early hydrogeological events. The estimate of the onset time of gas-phase generation, as early as about 140 Ma in the Williston Basin, further provides information about the proportion of He fluxing the sedimentary system that may have accumulated in the reservoir gas phase and, together with system specific geological and hydrogeological information, can be applied to assist He exploration in similar sedimentary regimes.

Online content

Any methods, additional references, Nature Portfolio reporting summaries, source data, extended data, supplementary information, acknowledgements, peer review information; details of author contributions and competing interests; and statements of data and code availability are available at https://doi.org/10.1038/s41586-022-05659-0.

1. Aggarwal, P. K. et al. Continental degassing of ^{4}He by surficial discharge of deep groundwater. *Nat. Geosci.* **8**, 35–39 (2015).
2. Andrews, J. et al. Radioelements, radiogenic helium and age relationships for groundwaters from the granites at Stripa, Sweden. *Geochim. Cosmochim. Acta* **46**, 1533–1543 (1982).
3. Sleep, N., Meibom, A., Fridriksson, T., Coleman, R. & Bird, D. H_2-rich fluids from serpentinisation: geochemical and biotic implications. *Proc. Natl Acad. Sci. USA* **101**, 12818–12823 (2004).
4. Lin, L.-H. et al. Long-term sustainability of a high-energy, low-diversity crustal biome. *Science* **314**, 479–482 (2006).
5. Sherwood Lollar, B., Onstott, T., Lacrampe-Couloume, G. & Ballentine, C. The contribution of the Precambrian continental lithosphere to global H_2 production. *Nature* **516**, 379–382 (2014).
6. Danabalan, D. et al. The principles of helium exploration. *Pet. Geosci.* https://doi.org/10.1144/petgeo2021-029 (2022).
7. Cheng, A. et al. Determining the role of diffusion and basement flux in controlling ^{4}He distribution in sedimentary basin fluids. *Earth Planet. Sci. Lett.* **574**, 117175 (2021).
8. Mamyrin, B. A. & Tolstikhin, I. N. *Helium Isotopes in Nature* (Elsevier, 2013).
9. Ballentine, C. J. & Burnard, P. G. Production, release and transport of noble gases in the continental crust. *Rev. Mineral. Geochem.* **47**, 481–538 (2002).

10. Lin, L.-H., Slater, G. F., Sherwood Lollar, B., Lacrampe-Couloume, G. & Onstott, T. C. The yield and isotopic composition of radiolytic H_2, a potential energy source for the deep subsurface biosphere. *Geochim. Cosmochim. Acta* **69**, 893–903 (2005).
11. Gold, T. & Held, M. Helium–nitrogen–methane systematics in natural gases of Texas and Kansas. *J. Pet. Geol* **10**, 415–424 (1987).
12. Ballentine, C. J. & Sherwood Lollar, B. Regional groundwater focusing of nitrogen and noble gases into the Hugoton-Panhandle giant gas field, USA. *Geochim. Cosmochim. Acta* **66**, 2483–2497 (2002).
13. Boreham, C. J. et al. Helium in the Australian liquefied natural gas economy. *APPEA J.* **58**, 209–237 (2018).
14. Kotarba, M. J. & Nagao, K. Composition and origin of natural gases accumulated in the Polish and Ukrainian parts of the Carpathian region: gaseous hydrocarbons, noble gases, carbon dioxide and nitrogen. *Chem. Geol.* **255**, 426–438 (2008).
15. Regenspurg, S. et al. Geochemical properties of saline geothermal fluids from the in-situ geothermal laboratory Groß Schönebeck (Germany). *Geochemistry* **70**, 3–12 (2010).
16. Hiyagon, H. & Kennedy, B. Noble gases in CH_4-rich gas fields, Alberta, Canada. *Geochim. Cosmochim. Acta* **56**, 1569–1589 (1992).
17. Jenden, P., Kaplan, I., Poreda, R. & Craig, H. Origin of nitrogen-rich natural gases in the California Great Valley: evidence from helium, carbon and nitrogen isotope ratios. *Geochim. Cosmochim. Acta* **52**, 851–861 (1988).
18. Li, L. et al. N_2 in deep subsurface fracture fluids of the Canadian Shield: source and possible recycling processes. *Chem. Geol.* **585**, 120571 (2021).
19. Karolytė, R. et al. The role of porosity in H_2/He production ratios in fracture fluids from the Witwatersrand Basin, South Africa. *Chem. Geol.* **595**, 120788 (2022).
20. Holland, G. et al. Deep fracture fluids isolated in the crust since the Precambrian era. *Nature* **497**, 357–360 (2013).
21. Warr, O. et al. Tracing ancient hydrogeological fracture network age and compartmentalisation using noble gases. *Geochim. Cosmochim. Acta* **222**, 340–362 (2018).
22. Warr, O., Giunta, T., Ballentine, C. J. & Sherwood Lollar, B. Mechanisms and rates of ^{4}He, ^{40}Ar, and H_2 production and accumulation in fracture fluids in Precambrian Shield environments. *Chem. Geol.* **530**, 119322 (2019).
23. Torgersen, T. Continental degassing flux of ^{4}He and its variability. *Geochem. Geophys. Geosyst.* **11**, Q06002 (2010).
24. Torgersen, T. & Clarke, W. Helium accumulation in groundwater, I: An evaluation of sources and the continental flux of crustal ^{4}He in the Great Artesian Basin, Australia. *Geochim. Cosmochim. Acta* **49**, 1211–1218 (1985).
25. Torgersen, T., Habermehl, M. & Clarke, W. Crustal helium fluxes and heat flow in the Great Artesian Basin, Australia. *Chem. Geol.* **102**, 139–152 (1992).
26. Castro, M. C., Goblet, P., Ledoux, E., Violette, S. & de Marsily, G. Noble gases as natural tracers of water circulation in the Paris Basin: 2. Calibration of a groundwater flow model using noble gas isotope data. *Water Resour. Res.* **34**, 2467–2483 (1998).
27. Byrne, D., Barry, P., Lawson, M. & Ballentine, C. The use of noble gas isotopes to constrain subsurface fluid flow and hydrocarbon migration in the East Texas Basin. *Geochim. Cosmochim. Acta* **268**, 186–208 (2020).
28. Lowenstern, J. B., Evans, W. C., Bergfeld, D. & Hunt, A. G. Prodigious degassing of a billion years of accumulated radiogenic helium at Yellowstone. *Nature* **506**, 355–358 (2014).
29. Bare, S. R. The Helium Crisis. *APS Phys.* https://www.aps.org/policy/analysis/helium-crisis.cfm (2016).
30. Gluyas, J. G. The emergence of the helium industry. The history of helium exploration, Part 1. *AAPG Explorer January 2019* 16–17 (2019).
31. Gluyas, J. G. Helium shortages and emerging helium provinces. The history of helium exploration, Part 2. *AAPG Explorer* February 2019 18–19 (2019).
32. Sorenson, R. P. J. A. B. A dynamic model for the Permian Panhandle and Hugoton fields, western Anadarko Basin. *AAPG Bull.* **89**, 921–938 (2005).
33. Ferguson, G. et al. The persistence of brines in sedimentary basins. *Geophys. Res. Lett.* **45**, 4851–4858 (2018).
34. Wang, X. et al. Radiogenic helium concentration and isotope variations in crustal gas pools from Sichuan Basin, China. *Appl. Geochem.* **117**, 104586 (2020).
35. Anderson, C. C. & Hinson, H. H. *Helium-Bearing Natural Gases of the United States: Analyses and Analytical Methods* Bulletin 486 (US Bureau of Mines, 1951).
36. Harris, D. C. & Baranoski, M. T. *Cambrian Pre-Knox Group Play in the Appalachian Basin* (Ohio Division of Geological Survey, 1997).
37. Mao, S. & Duan, Z. A thermodynamic model for calculating nitrogen solubility, gas phase composition and density of the N_2–H_2O–NaCl system. *Fluid Phase Equilib.* **248**, 103–114 (2006).
38. Yurkowski, M. M. *Helium in Southwestern Saskatchewan: Accumulation and Geological Setting* Open File Report 1 (Saskatchewan Ministry of the Economy, Saskatchewan Geological Survey, 2016).
39. Danabalan, D. *Helium: Exploration Methodology for a Strategic Resource* (Durham Univ., 2017).
40. Thompson, J. The occurrence of helium in the Cambrian near Swift Current, Saskatchewan. *Third International Williston Basin Symposium* 179–184 (1964).
41. Snyder, G. L. *Map of Precambrian and adjacent Phanerozoic rocks of the Hartville uplift, Goshen, Niobrara, and Platte counties, Wyoming* Report No. 2331-1258 (1980).
42. Munnerlyn, R. D. & Miller, R. D. *Helium-Bearing Natural Gases of the United States: Analyses, Second Supplement to Bulletin 486* Bulletin 617 (US Bureau of Mines, 1963).
43. Bachu, S. & Hitchon, B. Regional-scale flow of formation waters in the Williston Basin. *AAPG Bull.* **80**, 248–264 (1996).
44. Zhu, C. & Hajnal, Z. Tectonic development of the northern Williston Basin: a seismic interpretation of an east-west regional profile. *Can. J. Earth Sci.* **30**, 621–630 (1993).

Methods

Deriving ^{4}He groundwater concentrations from natural gas samples

Twenty-seven gas samples from different stratigraphic horizons (Cretaceous to the Cambrian) in the Williston Basin were collected for noble gas isotopic and gas composition (Extended Data Table 2)[7]. The original ^{4}He concentration in groundwater before degassing can be estimated as:

$$^4\mathrm{He}_{\mathrm{groundwater}} = {}^{20}\mathrm{Ne}_{\mathrm{asw}} \times \left(\frac{^4\mathrm{He}}{^{20}\mathrm{Ne}}\right)_{\mathrm{g}} \quad (1)$$

where $^4\mathrm{He}_{\mathrm{groundwater}}$ is the concentration of ^{4}He in groundwater before degassing, $^{20}\mathrm{Ne}_{\mathrm{asw}}$ is the concentration in air-saturated seawater and $\left(\frac{^4\mathrm{He}}{^{20}\mathrm{Ne}}\right)_{\mathrm{g}}$ is the ratio measured from gas samples (Extended Data Table 2)[7]. The ^{20}Ne concentration in this water (seawater (salinity 35‰) at 298 K at 1-atm pressure) can be calculated from Henry's law as 1.33×10^{-7} cm^3 ^{20}Ne STP cm^{-3} water (H_2O), where cm^3 STP refers to the volume of the gas at standard temperature and pressure.

Modelling in situ and basement helium flux in a developing sedimentary basin

A vertical one-dimensional model is constructed from first principles to be compared with sample observations. The model allows each stratigraphic unit to be added incrementally at the start of the formation age and interactively calculates the evolution of the dissolved He concentration in the water-filled pore spaces as a function of depth and time. The model accounts for both in situ radiogenic ^{4}He production and ^{4}He flux from the Precambrian basement.

^{4}He transport is governed by the following equation

$$\phi\frac{\partial C}{\partial t} + q\frac{\partial C}{\partial z} = D_{\mathrm{e}}\frac{\partial^2 C}{\partial z^2} + \phi p \quad (2)$$

where ϕ is the rock porosity, C is the mass concentration of the solute, t is time, z is the distance from the crystalline basement, p is the production rate per volume of rock and q is the average linear velocity. For diffusion-only scenarios, $q = 0$. D_{e} is the effective diffusion coefficient and is defined according to Fick's first law

$$J_{\mathrm{d}} = -D_{\mathrm{e}}\frac{\partial C}{\partial z} \quad (3)$$

where J_{d} is the diffusive mass flux rate. The parameters used for transport modelling, including porosities, U and Th concentrations, diffusion coefficients, compaction and isopach thickness, are from ref. [44].

The basement ^{4}He flux fitting the observed ^{4}He distribution is between 0.8 mol ^{4}He m^{-2} yr^{-1} and 1.6×10^{-6} mol ^{4}He m^{-2} yr^{-1} (available in ref. [7]) and is comparable to the steady-state flux estimated for the average continental crust (1.47×10^{-6} mol ^{4}He m^{-2} yr^{-1})[19]. ^{4}He-depleted lithologies (Fig. 2a) are consistent with a history of water flooding and produced water disposal in shallow aquifers by decades of hydrocarbon industry exploration (Extended Data Fig. 1).

Basin model porosity changes during geological time

The Williston Basin is an oval intracratonic basin overlying a Precambrian crystalline basement with sediments preserved as a result of episodic subsidence throughout the Palaeozoic[44], cycles of proto-Pacific connection[43,45] and progressive uplift forming a clastic, shale-dominated foreland basin[46,47].

The model incorporates sediment compaction, which is calculated based on standard effective stress[48] using BPA-CAULDRON, a proprietary program owned by the Shell oil company[7]. Porosity reduction is considered as a time-step function that happens when the next unit is deposited. The reduction of pore space at each step is assumed within the model to displace pore-water laterally and therefore has a negligible effect on dissolved-gas concentrations in the residual pore water.

Including exsolution of nitrogen in the model

To investigate the effect of N_2 gas formation in the distribution of He in the sedimentary column, the model considers the diffusion of N_2 in parallel with He. Model air-saturated-water N_2 is 0.012 cm^3 cm^{-3} H_2O (ref. [37]; seawater at 298 K at 1-atm pressure), and trivial at depth (Fig. 2b). The diffusion coefficient of N_2 is, like He, dominantly controlled by temperature[49]. $D_{\mathrm{N_2}}^{\mathrm{water}}$ is approximately linearly proportional to temperature (T, in K). The extrapolated linear correlation is

$$D_{\mathrm{N_2}}^{\mathrm{water}} = 6.83 \times 10^{-9} T - 1.86 \times 10^{-6} \quad (4)$$

in cm^2 s^{-1}.

At each time step, the model first updates the N_2, He and Ne concentration profiles considering a diffusive transport following steps and factors discussed in 'Modelling in situ and basement helium flux in a developing sedimentary basin'.

The N_2 gas solubilities are calculated following the thermodynamic model determined by ref. [37] for N_2–H_2O–NaCl water systems. These are nonlinear and calculated for reservoir temperature and pressure, which increases with depth, and the salinity of the corresponding unit:

$$m_i = y_i P\left[\exp\left(\frac{\mu_i^{l(0)}}{RT} - \ln\varnothing_i + 2\lambda_{i,\mathrm{Na}} m_{\mathrm{NaCl}} + \varepsilon_{i,\mathrm{Na,Cl}} m_{\mathrm{NaCl}}^2\right)\right]^{-1}$$

where, i refers to N_2 in the corresponding system (in this scenario, we consider the N_2–H_2O–NaCl system), y_i is the mole fraction of i in the gas phase, m_i is the molality mol kg^{-1} of i in the liquid phase, P is the total pressure (bar), that is, $P_i + P_{\mathrm{H_2O}}$, where $P_{\mathrm{H_2O}}$ is the pressure of water vapour, $\varnothing_i$ is the fugacity coefficient of i, $\mu_i^{l(0)}$ is chemical potential in a hypothetically ideal solution of unit molality, where l indicates liquid and (0) refers to the standard state, and λ_i and ε_i are second-order and third-order interaction parameters, respectively. y_i, the mole fraction of N_2 in the gas phase, $y_{\mathrm{N_2}}$, can be calculated assuming that water vapour is the only other gas content in the system

$$y_i = 1 - y_{\mathrm{H_2O}} \quad (5)$$

All parameters used for calculations are summarized by ref. [37].

The N_2 diffusion profile with a 1-m resolution is compared point to point with the solubilities calculated to identify depths where N_2 exceeds saturation and forms a gas phase. For those depths where a gas phase is formed, the groundwater N_2 concentration is then set to the solubility values at the corresponding depth, and the excess N_2 forms a gas phase. The corresponding gas–water ratio can be calculated. The gas phase then extracts He and Ne from the groundwater. The He and Ne concentrations from the diffusive profiles will equilibrate between the gas and water phase based on Henry's constant. Overall, when a gas phase is formed, the N_2, He and Ne profiles in the groundwater will be updated and the gas phase content is calculated.

Then, at the next time step, again, the first calculation is to establish new diffusive profiles from the groundwater concentrations concluded at the previous time step and considering the accumulation of N_2, He and Ne from their sources between the time steps ('Modelling in situ and basement helium flux in a developing sedimentary basin'). The model then compares the sum of N_2 in the groundwater and the gas phase (exsolved from the previous time step) at each depth with the corresponding solubility. If the N_2 budget (sum of N_2 dissolved in water and in gas) is greater than the solubility, the groundwater concentration

is set to its solubility at the depth and the amount that exceeds solubility forms a new gas phase. The total amount of He and Ne at each depth are calculated and then redistributed between the new gas and water phases. The model takes another path if the N_2 budget (sum of N_2 dissolved in water and in gas) is smaller than the solubility. When this happens, the gas phase disappears and the groundwater N_2 concentration is then the sum of the N_2 content in both the water and the gas phases, which simulates the re-dissolution of N_2 gas back to the water phase. If re-dissolution happens, He and Ne are also redissolved simultaneously, updating the He and Ne concentrations in the groundwater system.

Model parameter sensitivity and key input parameter ranges considered in the sensitivity assessment

Time resolution. The model with a ^{4}He basement flux of 1.6×10^{-6} mol m^{-2} yr^{-1} and a basement $N_2/^4$He ratio of 50 was run with time steps of 1 Ma, 0.1 Ma, 0.05 Ma and 0.01 Ma, to test the sensitivity of the model response to higher time resolution. The test results are presented in Extended Data Table 3. Although the estimated gas volume increases with a higher temporal resolution, the gas volume estimation, ^{4}He concentration, $N_2/^4$He and ^{4}He/^{20}Ne in the dissolved-gas phase show exponentially converging trends with higher time resolutions. Models with a time resolution of 0.1 Ma provide good modelling results for the purpose of the paper.

Basin-wide groundwater re-set sensitivity to hydrogeological events. The model with ^{4}He basement flux of 1.6×10^{-6} mol m^{-2} yr^{-1} and a basement $N_2/^4$He ratio of 50 was run starting from 500 Ma (default), 300 Ma, 200 Ma and 100 Ma to simulate the model sensitivity to past basinal hydrogeological events. The 500-Ma model starts diffusive transport since the deposition of the oldest unit in the basin and assumes no perturbation of water during the past 500 Ma. To simulate a basin-wise complete water turnover event, the entire sedimentary column is re-set with air-saturated water at t = 300 Ma, t = 200 Ma and t = 100 Ma. These values are arbitrary. In all scenarios, a gas phase is predicted with V_g/V_l of 0.0478, 0.0474, 0.0422 and 0.0251, with estimated gas-phase formation time starting from 145 Ma, 143 Ma, 131 Ma and 65 Ma for 500 Ma (default), 300 Ma, 200 Ma and 100 Ma, respectively. All models give comparable ^{4}He concentration, $N_2/^4$He and ^{4}He/^{20}Ne. It is therefore suggested that for this basin architecture, hydrogeological events more than 200 Ma ago do not play a major role in delaying the formation of gas pools.

Basement nitrogen and helium flux. To investigate the model sensitivity response to the basement N_2 and He flux, the model was run for 31 He flux values, from 0 to 3×10^{-6} mol m^{-2} yr^{-1} with an interval of 0.1×10^{-6} mol m^{-2} yr^{-1}, and 11 $N_2/^4$He values, from 10 to 60 with an interval of 5. The modelled ^{4}He concentrations, $N_2/^4$He ratios, ^{20}Ne/^{4}He ratios in the gas phase and gas–water ratios (V_g/V_l) in the Cambrian Deadwood Formation are plotted for different combinations of ^{4}He flux and $N_2/^4$He flux ratios (Extended Data Fig. 2). The contour maps can be compared with the observation from the Cambrian Deadwood Formation for the best estimate of basement $N_2/^4$He ratios. With an estimated ^{4}He basement flux of 0.8×10^{-6}–1.6×10^{-6} mol ^{4}He m^{-2} yr^{-1}, the range of basement $N_2/^4$He ratios is between 30 and 50.

Data availability

All data are previously published and available in ref. [7], with data tables uploaded to an open-source repository at https://doi.org/10.5281/zenodo.7267734. Source data are provided with this paper.

Code availability

The code for the numerical model developed for this paper can be accessed on an open-source repository at https://doi.org/10.5281/zenodo.7271773.

45. Kent, D. in *Geological Atlas of the Western Canada Sedimentary Basin* (eds Mossop, G. D. & Shetsen, I.) 69–86 (Canadian Society of Petroleum Geologists and Alberta Research Council, 1994).
46. Price, R. in *Geological Atlas of the Western Canada Sedimentary Basin* (eds Mossop, G. D. & Shetsen, I.) 13–24 (Canadian Society of Petroleum Geologists and Alberta Research Council, 1994).
47. Wright, G., McMechan, M. & Potter, D. in *Geological Atlas of the Western Canada Sedimentary Basin* (eds Mossop, G. D. & Shetsen, I.) 25–40 (Canadian Society of Petroleum Geologists and Alberta Research Council, 1994).
48. Terzaghi, K. *Theoretical Soil Mechanics* 11–15 (Wiley, 1943).
49. Cadogan, S. P., Maitland, G. C. & Trusler, J. M. Diffusion coefficients of CO_2 and N_2 in water at temperatures between 298.15 K and 423.15 K at pressures up to 45 MPa. *J. Chem. Eng. Data* **59**, 519–525 (2014).
50. Sherwood Lollar, B., Weise, S., Frape, S. & Barker, J. Isotopic constraints on the migration of hydrocarbon and helium gases of southwestern Ontario. *Bull. Can. Petrol. Geol.* **42**, 283–295 (1994).
51. Sherwood Lollar, B. et al. Unravelling abiogenic and biogenic sources of methane in the Earth's deep subsurface. *Chem. Geol.* **226**, 328–339 (2006).
52. Telling, J. et al. Bioenergetic constraints on microbial hydrogen utilisation in Precambrian deep crustal fracture fluids. *Geomicrobiol. J.* **35**, 108–119 (2018).
53. Onstott, T. C. et al. The origin and age of biogeochemical trends in deep fracture water of the Witwatersrand Basin, South Africa. *Geomicrobiol. J.* **23**, 369–414 (2006).
54. Heard, A. W. et al. South African crustal fracture fluids preserve paleometeoric water signatures for up to tens of millions of years. *Chem. Geol.* **493**, 379–395 (2018).
55. Ward, J. et al. Microbial hydrocarbon gases in the Witwatersrand Basin, South Africa: implications for the deep biosphere. *Geochim. Cosmochim. Acta* **68**, 3239–3250 (2004).

Acknowledgements This study was supported by funding from China Scholarship Council, the Oxford Department of Earth Sciences, the Natural Sciences and Engineering Research Council of Canada, and the NERC Centre for Doctoral Training in Oil and Gas. C.J.B. and B.S.L. are fellows of the CIFAR Earth 4D Subsurface Science and Exploration programme.

Author contributions Conceptualization: C.J.B., B.S.L., J.G.G. and A.C. Methodology: A.C., C.J.B. and B.S.L. Formal analysis and investigation: A.C. Software: A.C. Visualization: A.C. and C.J.B. Writing—original draft preparation: A.C. Writing—review and editing: A.C., C.J.B., B.S.L. and J.G.G. Funding acquisition: C.J.B. and B.S.L. Supervision: C.J.B. and B.S.L. All authors reviewed the results and approved the final version of the manuscript.

Competing interests The authors declare no competing interests.

Additional information

Supplementary information The online version contains supplementary material available at https://doi.org/10.1038/s41586-022-05659-0.

Correspondence and requests for materials should be addressed to Anran Cheng or Chris J. Ballentine.

Peer review information *Nature* thanks Werner Aeschbach and the other, anonymous, reviewer(s) for their contribution to the peer review of this work. Peer reviewer reports are available.

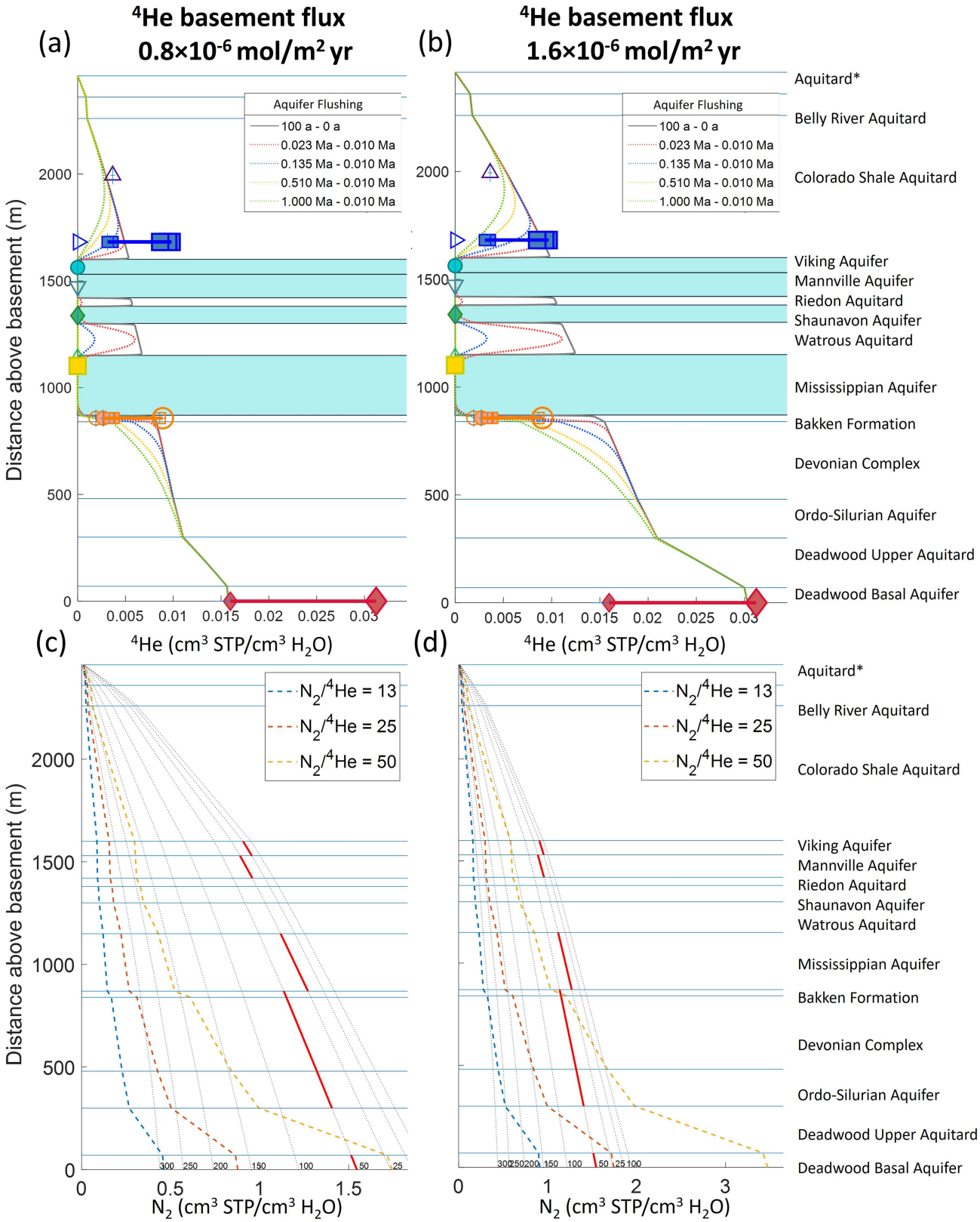

Extended Data Fig. 1 | See next page for caption.

Extended Data Fig. 1 | Examples of diffusive concentration profiles of helium and nitrogen with the diffusion-only model. The diffusive concentration profiles of helium (**a,b**) from the diffusion-only model are shown for a basement flux of 0.8×10^{-6} mol ^{4}He m^{-2} yr^{-1} and 1.6×10^{-6} mol ^{4}He m^{-2} yr^{-1}. The concentration profiles presented are modelled results considering several aquifer flushing events in the past million years (natural recharge and anthropogenic flooding)[7]. For each helium flux value, the nitrogen profiles modelled are with $N_2/^4$He basement flux ratios of 13, 25 and 50, respectively (**c,d**) with the diffusion-only model. The horizontal lines are the boundaries of lithological units. The dotted black lines are the solubility of nitrogen over a range of salinities (labelled to the right of each line). From right-most to the left, the lines correspond to salinities of 0, 10, 25, 50, 100, 150, 200, 250 and 300‰ respectively. The solid red lines represent the saturation limit for different formation waters estimated from salinity maps produced by ref. [43]. If the predicted nitrogen concentration for a particular ^{4}He flux and basement $N_2/^4$He exceeds solubility (that is, the coloured concentration line is higher than the solid red line), a nitrogen gas phase is predicted. When helium basement flux is 0.8×10^{-6} mol ^{4}He m^{-2} yr^{-1}, gas is predicted to form only in the basal units when $N_2/^4$He is 50. As demonstrated in the figure, when helium basement flux is 1.6×10^{-6} mol ^{4}He m^{-2} yr^{-1}, gas is predicted to develop in the bottom unit when $N_2/^4$He is 25 and in units from Cambrian up to Devonian when $N_2/^4$He is 50.

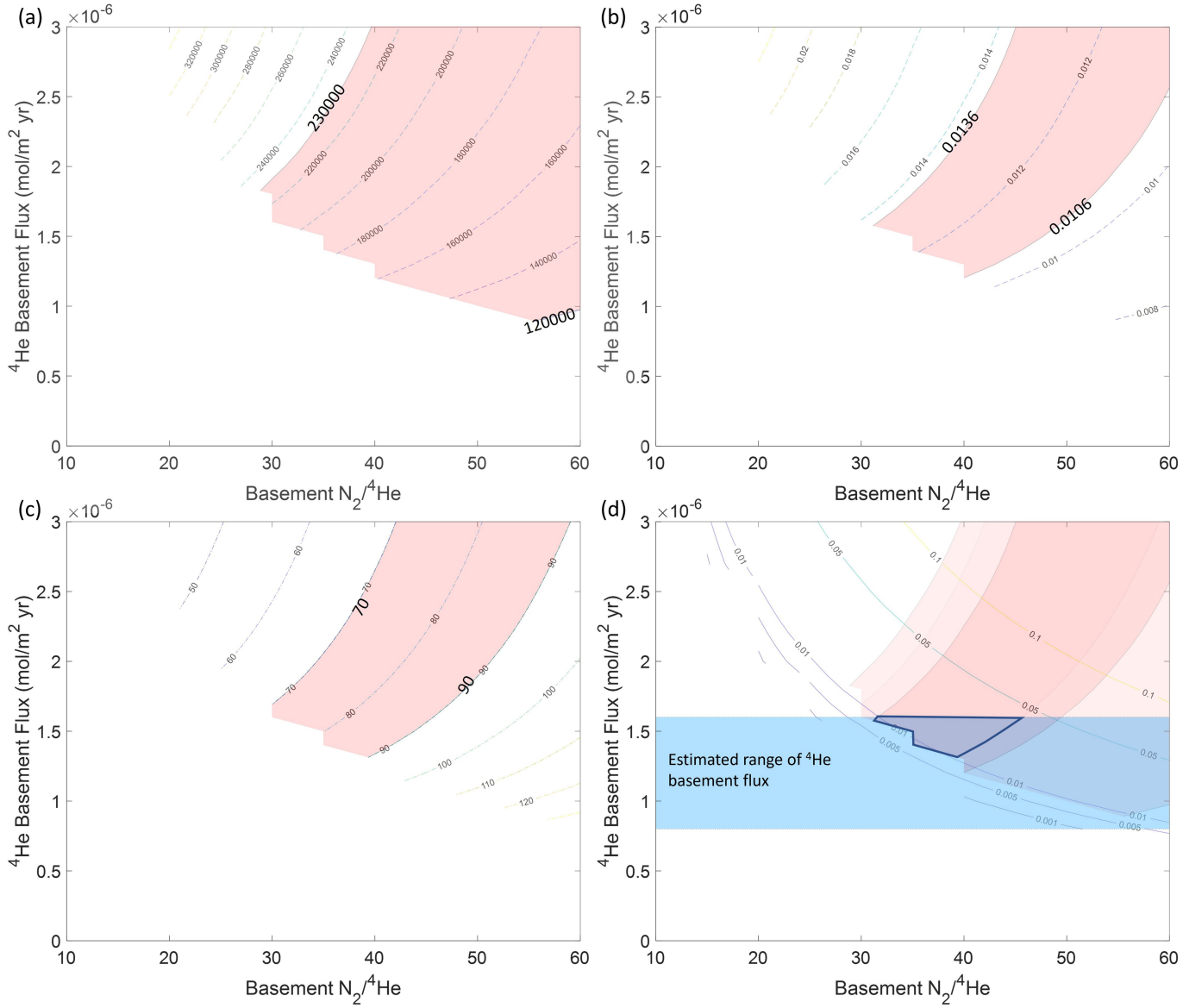

Extended Data Fig. 2 | Gas composition obtained from diffusion and exsolution model over a range of basement helium and $N_2/^4He$ flux. The plots present the modelled (**a**) $^4He/^{20}Ne$ ratios, (**b**) ^4He concentration, (**c**) $N_2/^4He$ ratios in the gas phase and gas–water ratio (V_g/V_l) in the Cambrian Deadwood Formation. The shaded areas are constrained by the lower and upper limits of the samples. By overlapping plots (**a**) (**b**) and (**c**), plot (**d**) demonstrates the best-estimated combinations of ^4He basement flux and $N_2/^4He$ ratios to be ^4He basement flux of 0.8×10^{-6}–1.6×10^{-6} mol ^4He m^{-2} yr^{-1} and basement $N_2/^4He$ ranges between 30 and 50.

Extended Data Table 1 | $N_2/^4He$ or N_2/He ratios of sedimentary basin fluids sampled proximal to the basement and samples from the crystalline basement refs. [11–13,15,18,32,34–36,50–55]

Location	$N_2/^4He$	Reference
Sedimentary units proximal to the basement		
Kanas-Hugoton-Panhandle, USA	13-50 (n=1069)	11,12
Sichuan Basin, China	12-227 (n=55)	35
Alberta Basin, Canada	10-67 (n=8)	33
Anardarko and Salina Basins, USA	12-29 (n=2)	36
Appalachian Basin, North America	44-54 (n=3)	37
Southwestern Ontario Basin, Canada	6-58 (n=18)	51
Amadeus Basin, Australia	10-25 (n=6) *	13
Crystalline Basement		
Kidd Creek, Canada	2-177 (n=85)	18
Copper Cliff South, Canada	0.1-8 (n=23)	18,52
Thompson Mine, Canada	11-44 (n=16)	18,53
Yellowknife, Canada	3-8 (n=6)	18
Birchtree, Canada	13-55 (n=4)	18
Nickel Rim, Canada	1.6-1.9 (n=4)	18
Driefontein, South Africa	0.2-1240 (n=28)	52,54,55
Evander, South Africa	1.3-1211 (n=22)	54,56
Beatrix, South Africa	0.1-377 (n=16)	54,56
Kloof, South Africa	0.6-16 (n=16)	52,54,56
Mponeng, South Africa	0.6-3 (n=9)	52,54
Masimong, South Africa	1.3-5 (n=3)	54-56
Merriespruit, South Africa	1.2-405 (n=3)	54,56
Tau Tona, South Africa	15-405 (n=2)	54,55
Middelbult, South Africa	49-239 (n=2)	56
Star Diamonds, South Africa	67(n=1)	55
Transvall, South Africa	237 (n=1)	55
Zondereind, South Africa	17(n=1)	55
Exploration borehole, South Africa	1-101 (n=10)	15

Extended Data Table 2 | ^{4}He and ^{20}Ne concentrations of gas samples collected in the Williston Basin and the estimated helium in groundwater before degassing

Sample name	Distance above basement (m)	N_2 %	$^{4}He \times 10^{-5}$ cm^3 STP/cm^3	$^{20}Ne \times 10^{-8}$ cm^3 STP/cm^3	$^{4}He_{water} \times 10^{-4}$ (cm^3 STP/cm^3 H_2O)
Milk River					
14-8-3-27W3	1733	3.8	96.2 ± 2.89	2.7 ± 0.17	46.9
2nd White Specks (Belle Plaine)					
11-9-17-23W2	1567	61.9	14.5 ± 0.43	46.6 ± 2.83	0.4
2nd White Specks (Alderson)					
8-31-15-14W4	1490	5.2	190.0 ± 2.15	8.8 ± 0.80	(28.4) **79.1**
5-31-15-14W4	1490	6.5	200.0 ± 2.22	9.0 ± 0.82	(29.3) **76.2**
14-31-15-14W4	1490	6.5	170.0 ± 1.90	8.9 ± 0.81	(25.1) **69.5**
Viking					
1-7-25-12W3	1357	26.4	26.6 ± 0.80	13.2 ± 0.80	2.7
7A-1-32-24-12W3	1412	32.9	10.2 ± 0.12	25.4 ± 2.33	0.5
16-30-23-12W3	1325	20.9	31.9 ± 0.96	13.4 ± 0.82	3.1
Mannville					
5-16-6-13W2(#6) b	1764	89.4	2050.0 ± 61.50	207.6 ± 12.59	13.1
5-16-6-13W2(#8) c	1764	78.9	2020.0 ± 60.60	273.3 ± 16.58	9.8
16-28-5-13W2 d	1764	74.6	1610.0 ± 48.30	1574.6 ± 95.54	1.4
5-16-6-13W2(#3) e	1764	86.6	1610.0 ± 48.30	583.9 ± 35.42	3.6
5-16-6-13W2(#6) f	1764	88.6	2020.0 ± 60.60	198.4 ± 12.04	13.5
5-16-6-13W2(#8) g	1764	81.8	2840.0 ± 85.20	196.4 ± 11.91	19.1
16-28-5-13W2 h	1764	87.4	2020.0 ± 60.60	1391.7 ± 84.43	1.9
Shaunavon					
15-10-7-19W3	993	9.4	38.0 ± 0.42	6.4 ± 0.58	7.9
4C-15-9-6-19W3	990	10.7	43.3 ± 0.49	6.3 ± 0.57	9.1
2B-3-28-6-19W3	980	11	54.8 ± 0.61	8.0 ± 0.73	9
Midale					
8-25-6-13W2	1364	0	2.8 ± 0.09	0.5 ± 0.03	8.2
2-25-6-13W2	1360	26	22.6 ± 0.68	229.4 ± 13.92	0.1
Frobisher					
2-32-5-13W2	1313	73.7	30.3 ± 0.34	23.0 ± 1.59	(1.8) **6.3**
Bakken (Weyburn)					
13-24-5-16W 2	717	12.7	146.0 ± 4.38	7.4 ± 0.45	105.3
1-21-5-16W2	1181	14.9	299.0 ± 8.97	21.4 ± 1.30	36.1
16-12-5-16W2	980	26.8	70.9 ± 1.15	3.6 ± 0.33	36.1
Bakken (Estevan)					
13-31-1-6W2	981	9.9	59.1 ± 1.77	0.8 ± 0.05	28.9
11-31-1-6W2	996	4.4	38.2 ± 0.66	1.6 ± 0.13	20.5
4-6-2-6W2	1000	3.5	28.8 ± 0.49	1.2 ± 0.10	28.7
Deadwood					
10-3-5-8W3	0	96.1	1390.0 ± 94.00	11.6 ± 0.88	(159.6) **312.2**

Mannville Formation (Cretaceous Aquifer) samples are gas exsolved from groundwater through a gas–water separator at the surface, while others are gas samples collected from borehole well heads. ^{4}He groundwater concentrations with air correction[7] are shown in bold and values before correction are in parentheses.

Extended Data Table 3 | Sensitivity tests for the diffusion and exsolution model with different time-step resolution and re-setting scenarios when the helium basement flux is 1.6×10^{-6} mol $^4He\ m^{-2}\ yr^{-1}$ and $N_2/^4He$ is 50

Model	V_g/V_l (Deadwood)	Gas forming (Ma)	^4He concentration (cc STP/cc) ×100	$N^2/^4He$	$^4He/^{20}Ne$
1Ma resolution – 500Ma	0.0478	145	1.01-1.11	92-99	164000
0.1Ma resolution – 500Ma	0.0544	144	1.04-1.12	90-96	160000
0.05Ma resolution – 500Ma	0.0548	144	1.04-1.12	90-96	160000
0.01Ma resolution – 500Ma	0.0551	153	1.04-1.07	94-96	160000
1Ma resolution – 300Ma	0.0474	143	1.02-1.11	91-99	164000
1Ma resolution – 200Ma	0.0422	131	1.03-1.13	90-97	166000
1Ma resolution – 100Ma	0.0251	65	1.05-1.15	88-95	169000